October 1, 2002

UCD-EXPH/021001
hep-ex/0210003

Electroweak Physics

Martin W. Grünewald

University College Dublin
Department of Experimental Physics
Belfield, Dublin 4
Ireland

Abstract

The status of precision electroweak measurements as of summer 2002 is reviewed. The recent results on the anomalous magnetic moment of the muon and on neutrino-nucleon scattering are discussed. Precision results on the electroweak interaction obtained by the experiments at the SLC, LEP and TEVATRON colliders are presented. The experimental results are compared with the predictions of the minimal Standard Model and are used to constrain its parameters, including the mass of the Higgs boson. The final LEP results on the direct search for the Higgs boson of the Standard Model are presented.

Plenary talk presented at the 31st International Conference on High Energy Physics, Amsterdam, The Netherlands, July 24-31, 2002

Electroweak Physics

Martin W. Grünewald[a]*

[a] Department of Experimental Physics, University College Dublin, Belfield, Dublin 4, Ireland

The status of precision electroweak measurements as of summer 2002 is reviewed. The recent results on the anomalous magnetic moment of the muon and on neutrino-nucleon scattering are discussed. Precision results on the electroweak interaction obtained by the experiments at the SLC, LEP and TEVATRON colliders are presented. The experimental results are compared with the predictions of the minimal Standard Model and are used to constrain its parameters, including the mass of the Higgs boson. The final LEP results on the direct search for the Higgs boson of the Standard Model are presented.

1. INTRODUCTION

In this paper the current status of the precision measurements of observables in electroweak physics are reviewed. In increasing energy scale, the main measurements consist of: the muon anomalous magnetic moment measured by the Brookhaven collaboration E821, neutrino-nucleon scattering measured by the NuTeV collaboration, the precise results on Z boson properties determined at the electron-positron colliders SLC and LEP-1, and results on W-boson properties determined at the TEVATRON and at LEP-2.

The measurements are compared with the expectations calculated in the framework of the minimal Standard Model (SM). Radiative corrections are extracted from the measurements and tested quantitatively, in particular by comparing predicted masses of top quark and W boson derived from radiative corrections with the results of the direct measurements. Based on the complete set of measurements, constraints are set on the mass of the SM Higgs boson. The final results on the direct search for the SM Higgs boson at LEP-2 are also presented.

2. ANOMALOUS MAGNETIC MOMENT OF THE MUON

The Brookhaven experiment E821 measures the anomalous magnetic moment of the muon, a_μ, by measuring the muon spin precession frequency, ω, in an external magnetic field, B:

$$(g_\mu - 2)/2 \quad = \quad a_\mu \; = \; (\omega m_\mu c)/(eB)\,, \qquad (1)$$

where the magnetic field B is measured with a proton NMR probe. Based on the data collected in 1999 [1], consisting of nearly 10^9 positrons from μ^+ decay, the time spectrum shown in Figure 1 is obtained, yielding the result:

$$10^{10} a_\mu \quad = \quad 11\,659\,202 \pm 15\,, \qquad (2)$$

to be compared with the expected value of $11\,659\,160 \pm 7$ in units of 10^{-10} calculated in the framework of the minimal SM. The expectation being lower by about 2.6 standard deviations compared to the experimental result caused great excitement because shifts in a_μ could signal new physics [2], *e.g.*, supersymmetry.

The SM expectation contains four contributions, graphically shown in Figure 2. The QED part is calculated in a perturbation series in terms of powers of α/π, the first order term being the Schwinger term $\alpha/2\pi$. This part, +11658471, is by far the dominant part, but still calculated with negligible uncertainty. Likewise, the weak part, +15 units, is known with negligible uncertainty, while it's size is comparable to the experimental uncertainty. The uncertainty on the prediction of a_μ is fully dominated by the hadronic vacuum polarisation, where estimates for the first-order contribution range from 692 to 699 units, with uncertainties of about 7 units. The E821 collaboration has chosen the calculation yielding the result at the lower edge of this range. The

*E-mail: Martin.Grunewald@cern.ch

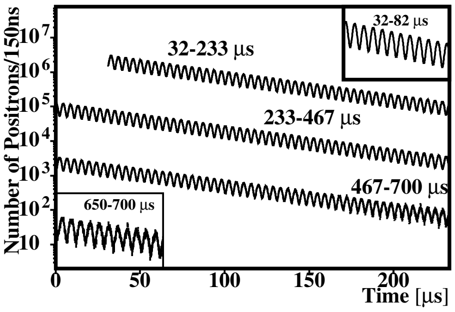

Figure 1. Counting rate recorded by E821 as a function of the muon decay time, modulated by the spin precession frequency ω.

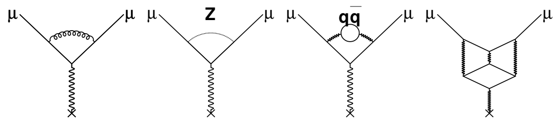

Figure 2. Feynman diagrams contributing to the anomalous magnetic moment of the muon. From left to right: QED, weak, hadronic vacuum polarisation and the light-by-light contribution.

second-order contribution is small, -10 ± 1 units. The hadronic light-by-light scattering contribution had been calculated to be -8 ± 4 units. Here, a sign error in the dominant contribution, the pion pole, has been discovered [3]. When corrected, this contribution changes to $+8 \pm 2$ units; the full SM prediction increases to $11\,659\,177 \pm 7$ units, reducing the difference between the experimental measurement and the theoretical calculation to 1.6 standard deviations.

On the last day of this conference, a new result of the E821 collaboration was presented based on the data collected in the year 2000 [4,5], corresponding to an additional $4 \cdot 10^9$ μ^+ decays:

$$10^{10} a_\mu = 11\,659\,204 \pm 8, \tag{3}$$

which dominates the new world average value of:

$$10^{10} a_\mu = 11\,659\,203 \pm 8. \tag{4}$$

The difference between theory and experiment is again at the level of 2.6 standard deviations.

Because of its large uncertainty, the first-order hadronic vacuum polarisation is under continued scrutiny. At this conference, new calculations were presented [6], predicting contributions even lower than the value of 692 used by E821. Clearly more work is needed to understand the large spread in the calculations, which should agree much better as they are all based on the same low energy data for electron-positron annihilations and τ decays into hadrons [7,8].

3. NEUTRINO NUCLEON SCATTERING

The NuTeV collaboration measures the electroweak mixing angle in t-channel neutrino-nucleon scattering as shown in Figure 3, involving charged current (CC) and neutral current (NC) reactions. Using for the first time both a neutrino and an anti-neutrino beam with high statistics, it is possible to exploit the Paschos-Wolfenstein relation [9]:

$$\begin{aligned} R_- &= \frac{\sigma_{NC}(\nu) - \sigma_{NC}(\bar{\nu})}{\sigma_{CC}(\nu) - \sigma_{CC}(\bar{\nu})} & (5) \\ &= 4 g_{L\nu}^2 \sum_{u,d} \left[g_{Lq}^2 - g_{Rq}^2 \right] & (6) \\ &= \rho_\nu \rho_{ud} \left[1/2 - \sin^2 \theta_W^{on-shell} \right] , & (7) \end{aligned}$$

where the sum runs over the valence quarks u and d. This relation holds for iso-scalar targets and up to small electroweak radiative corrections. Thus R_- is a measurement of the on-shell electroweak mixing angle. In the ideal case this measurement is insensitive to the effects of sea quarks, which cancel. Charm production, uncertain due to charm mass effects, enter only through CC scattering off valence d quarks, a CKM suppressed process.

Using a muon (anti-) neutrino beam, CC reactions contain a primary muon in the final state, while NC reactions do not. As shown in Figure 4, the muon as a minimum ionising particle traverses the complete detector, while the hadronic shower is confined in a small target volume. The length of the event thus discriminates clearly between CC and NC events.

The distributions of event lengths as observed for neutrino and anti-neutrino beams are shown in Figure 5. In total, close to 2 million events were

Figure 3. Feynman diagrams in νN scattering at parton level. Left: CC, right: NC interactions.

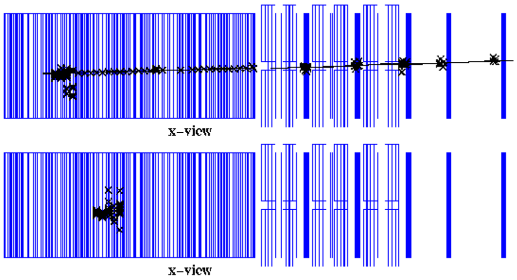

Figure 4. Events observed in the NuTeV detector. Top: CC event, bottom: NC event.

recorded by the NuTeV collaboration, 1167K CC and 457K NC events with neutrino beams, and 250K CC and 101K NC events with anti-neutrino beams. The separation between CC and NC events is dependent on the energy of the hadronic shower and ranges from 16 to 18 in units of counters (equivalent to 10 cm of steel) as indicated in the inserts of Figure 5.

In order to extract R_- from the measured distributions, a Monte Carlo simulation of the spectra of the (anti-) neutrino beams, radiative corrections and detector response is used. In terms of the on-shell electroweak mixing angle, NuTeV's final results reads [10]:

$$\begin{aligned}\sin^2\theta_W^{on-shell} &\equiv 1 - M_W^2/M_Z^2 \\ &= 0.2277 \pm 0.0013 \pm 0.0009 \\ &\quad -0.00022\frac{M_t^2-(175\ \mathrm{GeV})^2}{(50\ \mathrm{GeV})^2} \\ &\quad +0.00032\ln(M_H/150\ \mathrm{GeV})\,,\end{aligned} \tag{8}$$

where the first error is statistical and the second is systematic. Here $\rho = \rho_{SM}$ is assumed. This result is in very good agreement with the previous world average of $0.2277 \pm 0.0024(exp.) \pm 0.0019(theo)$ updated for the latest charm mass [11], as shown in Figure 6.

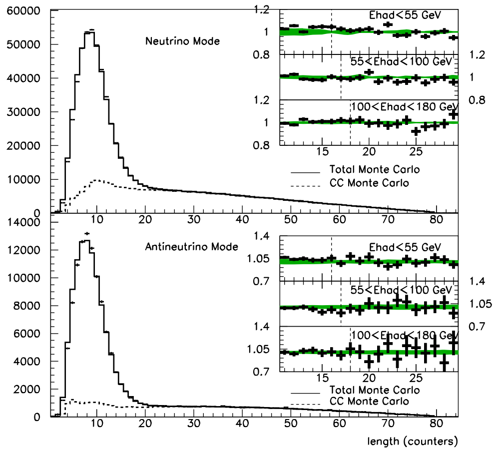

Figure 5. Distribution of event lengths.

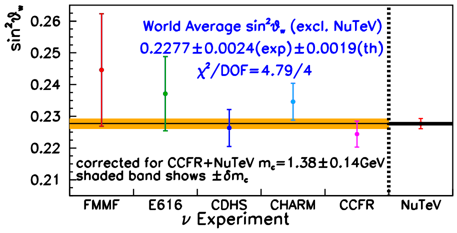

Figure 6. Comparison of results on the on-shell electroweak mixing angle in νN experiments.

The two contributions to the total systematic uncertainty of 0.0009 are about equal, 0.0006 each for experimental systematics and for modelling. The experimental systematics are dominated by the uncertainty on the (anti-)electron neutrino flux, as for such beams both CC and NC interactions lead to final states without primary muons. The model systematics are dominated by charm production and the strange-quark sea, effects which are much reduced compared to previous single-beam experiments. With a statistical error of 0.0013 and a total systematic error of 0.0009, NuTeV's final result is statistics limited.

Also this result caused a great deal of excitement, as the global SM analysis of all electroweak measurements, presented later in this paper, predicts a value of 0.2227 ± 0.0004 for the on-shell

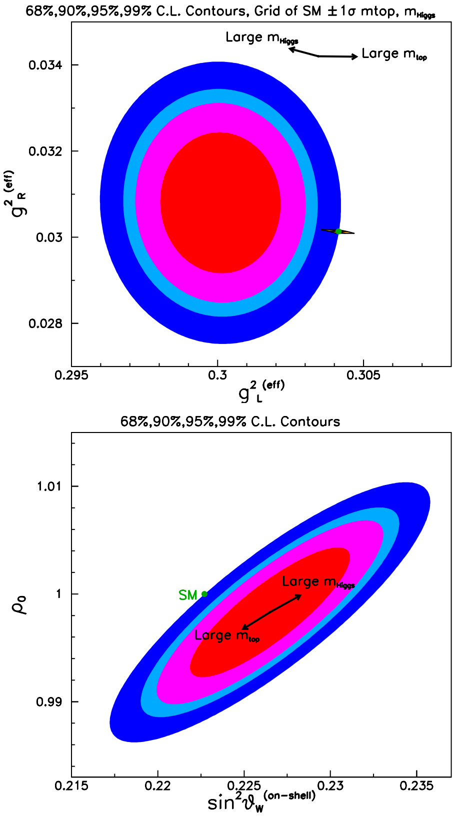

Figure 7. NuTeV result in the plane of effective right- and left-handed couplings (top) and of on-shell angle versus ρ-scale factor ρ_0.

electroweak mixing angle, showing a deviation from the NuTeV result at the level of 3.0 standard deviations.

In a more model-independent analysis, the NuTeV result is also interpreted in terms of effective left- and right-handed couplings, shown in Figure 7, defined as: $g^2_X(eff) = 4g^2_{L\nu}\sum_q g^2_{Xq}$ for $X = L, R$. Here the deviation is confined to the effective left-handed coupling product. Modifying all ρ parameters by a scale factor ρ_0, also shown in Figure 7, shows that either ρ_0 or the mixing angle, but not both, could be in agreement with the SM. Assuming the electroweak mixing angle to have it's expected value, the change in the ρ factors can be absorbed in ρ_ν, *i.e.*, interpreted as a change in the coupling strength of neutrinos, then lower than expected by about $(1.2 \pm 0.4)\%$. A similar trend is observed with the neutrino coupling as measured by the invisible width of the Z boson at LEP-1, yielding a much less significant deficit of $(0.5 \pm 0.3)\%$ in ρ_ν.

To date, various explanations ranging from old and new physics effects have been put forward and reviewed at this conference [12]. Some old physics effects are: theoretical uncertainties in PDFs, iso-spin violating PDFs, quark-antiquark asymmetries for sea quarks, nuclear shadowing asymmetries between W and Z interactions, etc. Some new physics effects are: a new heavy Z boson, contact interactions, lepto-quarks, new fermions, neutrinos oscillations, etc. Most of the old and new physics effects are, however, severely constrained by NuTeV itself or other precision electroweak measurements, thus cannot explain the full effect. As was pointed out at this conference, PDFs should be investigated, in particular the partly leading-order analysis employed by NuTeV should be assessed and eventually improved to next-to-leading order.

4. Z-BOSON PHYSICS

In the last decade, electron-positron annihilations at high energies have allowed to measure precisely a wealth of electroweak observables related to on-shell Z bosons decaying to fermion-antifermion pairs. The lowest-order Feynman diagrams contributing to fermion-pair production are shown in Figure 8. Figure 9 shows the total cross section for hadron production as a function of the e^+e^- centre-of-mass energy. Prominent features are the $1/s$ fall off at low energies due to virtual photon exchange, and the dominant Z resonance at 91 GeV. Also shown is the threshold for W^+W^- production around 160 GeV.

The properties of the Z boson are measured precisely by the SLC experiment SLD, and the LEP experiments ALEPH, DELPHI, L3 and OPAL. For example [13], the mass and width of the Z boson are $M_Z = 91187.5 \pm 2.1$ MeV, and $\Gamma_Z = 2495.2 \pm 2.3$ MeV. The number of light neutrinos species is found to be 2.9841 ± 0.0083, about 1.9 standard deviations smaller than three as already observed in the previous section.

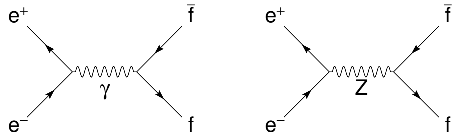

Figure 8. Feynman diagrams in $f\overline{f}$ production. Left: photon exchange; right: Z boson exchange.

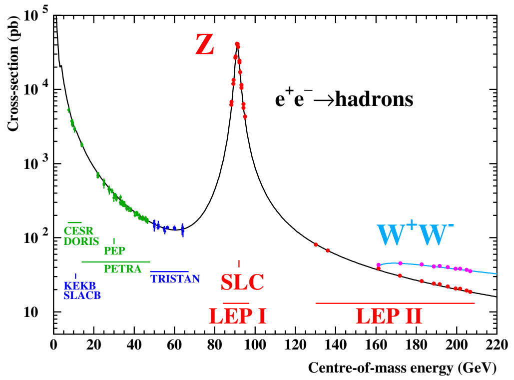

Figure 9. Hadron production in e^+e^- annihilation.

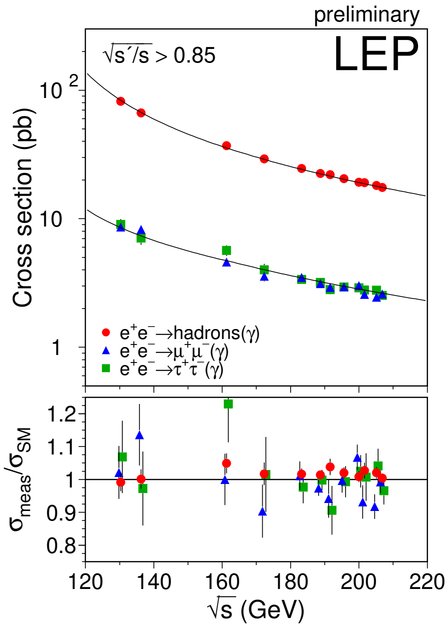

Figure 10. Measured cross sections for $f\overline{f}$ production at energies above the Z-pole, compared to the SM expectation.

4.1. Photon-Z Interference

Owing to the increase in centre-of-mass energy at LEP-2, fermion-pair production is now tested at energies much higher than the Z pole. The results from the LEP experiments, still preliminary, are combined taking common systematic uncertainties into account [14]. The combined cross sections are shown in Figure 10 and compared to the SM expectation. Besides searches for new physics, these data are used to determine the interference term between photon and Z-boson exchange for the hadronic final state. This is interesting and important because this interference term is fixed to its SM value when extracting the Z-boson mass quoted above from the LEP-1 Z-pole measurements. The situation is shown graphically in Figure 11. Relaxing the SM constraint on the hadronic interference term, the LEP-1 data alone shows a large correlation with M_Z, increasing the uncertainty on M_Z. Including the LEP-2 data constrains the interference term. The error on M_Z is reduced close to that obtained in the LEP-1 analysis with fixed interference term. Similar analysis are possible with data collected below the Z pole, *e.g.*, by TOPAZ [15] and VENUS [16] at TRISTAN, albeit with larger uncertainties.

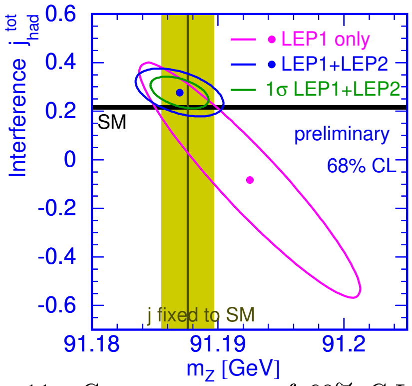

Figure 11. Contour curves of 68% C.L. in the plane of Z mass versus interference term for the hadronic final state.

The forward-backward asymmetries as mea-

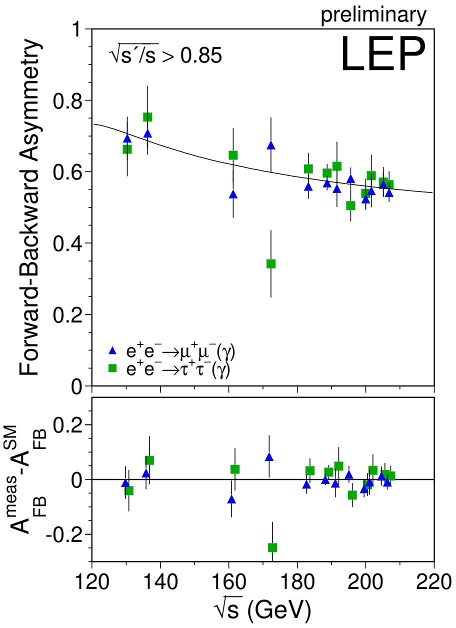

Figure 12. Measured forward-backward asymmetries for $f\overline{f}$ at energies above the Z-pole, compared to the SM expectation.

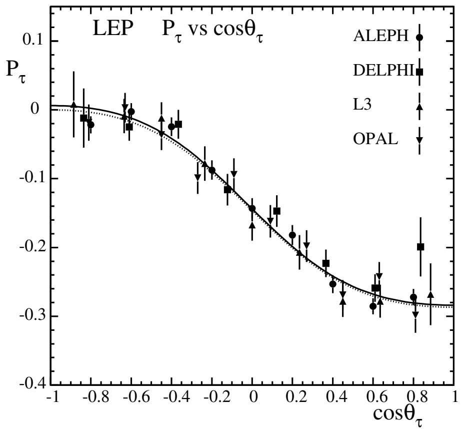

Figure 13. Tau polarisation as a function of the polar scattering angle in tau-pair production at LEP-1. The results of a fit to the data, with or without assuming e-τ universality, are shown as the dashed and solid line.

sured at energies above the Z-pole are shown in Figure 12. Analyses are currently ongoing to extract the γ/Z interference terms for leptons and for forward-backward asymmetries.

4.2. Leptonic Polarisation Asymmetries

In terms of the effective vector and axial-vector coupling constants, g_{Vf} and g_{Af}, the asymmetry parameter A_f is defined as:

$$A_f = 2\frac{g_{Vf}/g_{Af}}{1+(g_{Vf}/g_{Af})^2}\,. \tag{9}$$

The leptonic asymmetry parameter is measured at SLC and at LEP-1 in various processes. Assuming lepton universality, well supported by the experimental results, the following final results are obtained when combining the experiments:

$$A_\ell = 0.1512 \pm 0.0042 \quad \text{f/b asymmetry} \tag{10}$$
$$A_\ell = 0.1465 \pm 0.0033 \quad \tau \text{ polarisation} \tag{11}$$
$$A_\ell = 0.1513 \pm 0.0021 \quad \text{l/r asymmetries}, \tag{12}$$

in good agreement and with a combined value of:

$$A_\ell = 0.1501 \pm 0.0016\,. \tag{13}$$

As an example, the measurement of of the τ polarisation as a function of polar scattering angle is shown in Figure 13. For backward scattering, zero average helicity is expected and observed, while for forward scattering the largest polarisation is obtained.

4.3. Effective Coupling Constants

The effective coupling constants of the neutral weak current are defined as:

$$g_{Vf} = \sqrt{\rho_f}\left(T_3^f - 2Q_f \sin^2\theta_{eff}^f\right) \tag{14}$$
$$g_{Af} = \sqrt{\rho_f}\,T_3^f, \tag{15}$$

where T_3^f, Q_f and $\sin^2\theta_{eff}^f$ are the third component of the weak iso-spin, the electric charge and the effective electroweak mixing angle of fermion f. While the asymmetry parameter determines g_{Vf}/g_{Af}, the partial Z decay width constrains $g_{Vf}^2 + g_{Af}^2$, allowing to disentangle g_{Vf} and g_{Af}.

The results are displayed in Figure 14. The three contours for the three charged lepton

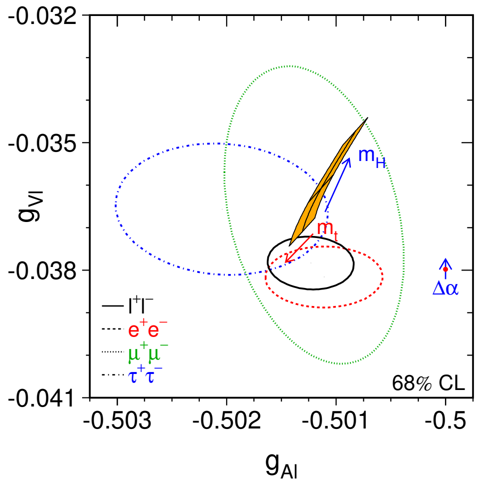

Figure 14. Contour curves of 68% C.L. in the $(g_{V\ell}, g_{A\ell})$ plane. The SM expectation is shown as the shaded area for $M_t = 174.3 \pm 5.1$ GeV and $M_H = 300^{+700}_{-186}$ GeV.

species e, μ and τ show lepton universality for both effective couplings. Under this assumption, the final Z-pole results are:

$$g_{V\ell} = -0.03783 \pm 0.00041 \quad (16)$$

$$g_{A\ell} = -0.50123 \pm 0.00026\,, \quad (17)$$

with a correlation of -5.9%.

Comparing the experimental contours with the predictions, non-QED electroweak radiative corrections are observed with a significance of 5 standard deviations. The results are in agreement with the expectations calculated in the framework of the minimal SM, and show preference for a light Higgs boson.

4.4. Heavy Flavour Results at the Z Pole

While the results on b- and c-quark production rates ($R_q = \Gamma_{qq}/\Gamma_{had}$) are final, several measurements of heavy-flavour asymmetries by SLD and at LEP are still preliminary, and thus is the joint combination of all heavy flavour results. The combined preliminary results on partial width ratios, forward-backward pole asymmetries $A^{0,f}_{fb} = 3/4 A_e A_f$, and forward-backward left-right asymmetries A_f are [17]:

$$R_b = 0.21644 \pm 0.00065 \quad (18)$$

$$R_c = 0.1718 \pm 0.0031 \quad (19)$$

$$A^{0,b}_{fb} = 0.0995 \pm 0.0017 \quad (20)$$

$$A^{0,c}_{fb} = 0.0713 \pm 0.0036 \quad (21)$$

$$A_b = 0.922 \pm 0.020 \quad (22)$$

$$A_c = 0.670 \pm 0.026\,, \quad (23)$$

with the largest correlation, +0.15, occurring between the b and c forward-backward asymmetries as shown in Figure 15. The value of the combined forward-backward b asymmetry prefers an intermediate Higgs-boson mass of a few hundred GeV.

The combination has a rather low χ^2 of 47.6 for $(105-14)$ degrees of freedom. The low χ^2 is mainly caused by two effects: for the rate measurements, several systematic uncertainties are studied by varying parameters in the MC simulation or evaluated from data. While no effect is observed, the statistical accuracy of the test is taken as a systematic uncertainty. In case of the asymmetries, all measurements are very consistent, as shown in Figures 16 and 17, although they as well as their combination are still statistics limited.

The mutual consistency of the measurements of A_q, $A^{0,q}_{fb} = (3/4)A_e A_q$ and A_ℓ assuming lepton universality is shown in Figure 18 for b quarks. Compared to the experimental uncertainties, the SM predictions are nearly constant in A_q, in contrast to the situation for A_ℓ. This is a consequence of the SM values of the electric charge and of the iso-spin for quarks.

Since the leptonic asymmetry parameter A_ℓ is already well determined, the measurements of $A^{0,q}_{fb}$ improve the determination of the quark asymmetry parameters A_q. In the combined analysis, all of the resulting asymmetry parameters A_f are decreased in value compared to their direct measurements, as shown by the contour curve in Figure 18. Compared to the SM expectation, the combined extracted value for A_b is lower by 2.6 standard deviations, while there is very good agreement for c quarks.

4.5. Effective Electroweak Mixing Angle

Assuming the SM structure of the effective coupling constants, the measurements of the various asymmetries are compared in terms of $\sin^2\theta^{\rm lept}_{\rm eff}$ in

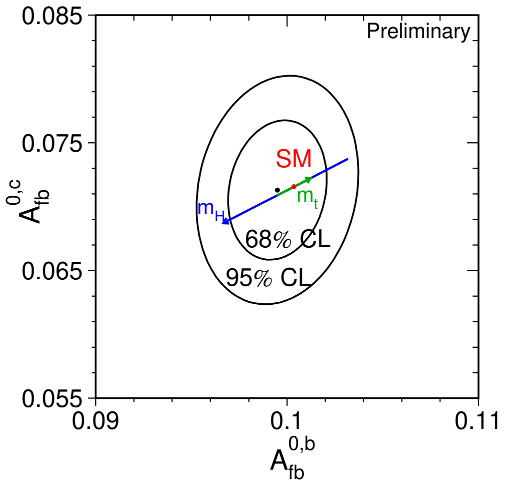

Figure 15. Contour curves of 68% C.L. in the $(\mathrm{A}_{\mathrm{fb}}^{0,\mathrm{b}}, \mathrm{A}_{\mathrm{fb}}^{0,\mathrm{c}})$ plane. The SM expectation is shown as the arrows for $M_{\mathrm{t}} = 174.3 \pm 5.1$ GeV and $M_{\mathrm{H}} = 300^{+700}_{-186}$ GeV.

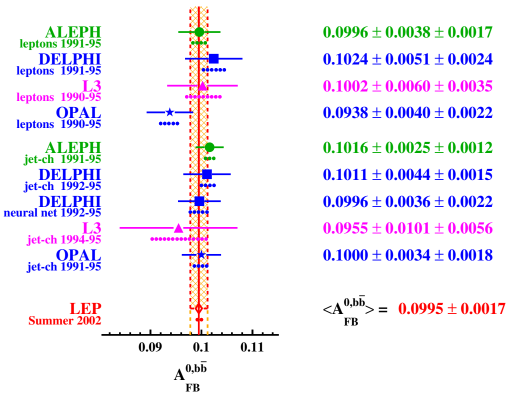

Figure 16. Measurements of $\mathrm{A}_{\mathrm{fb}}^{0,\mathrm{b}}$ at the Z pole.

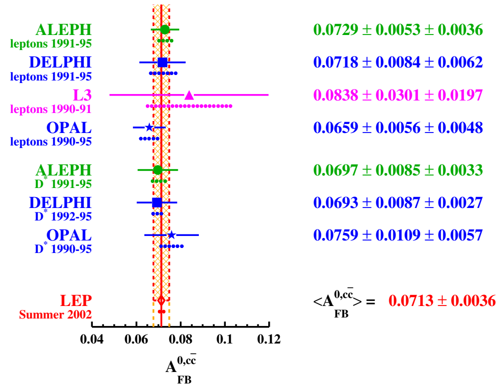

Figure 17. Measurements of $\mathrm{A}_{\mathrm{fb}}^{0,\mathrm{c}}$ at the Z pole.

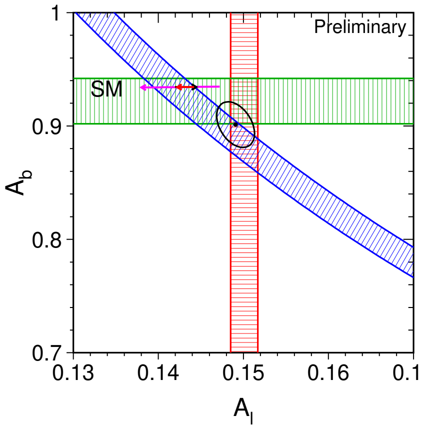

Figure 18. Bands of ± 1 standard deviation width showing the combined results of A_ℓ, A_b, and $\mathrm{A}_{\mathrm{fb}}^{0,\mathrm{b}}$. The SM expectation is shown as the arrows for $M_{\mathrm{t}} = 174.3 \pm 5.1$ GeV and $M_{\mathrm{H}} = 300^{+700}_{-186}$ GeV.

Figure 19. The measurements fall into two sets of three results each. In the first set, the results on $\sin^2\theta_{\mathrm{eff}}^{\mathrm{lept}}$ are derived from measurements depending on leptonic couplings only, $\mathrm{A}_{\mathrm{fb}}^{0,\ell}$, $\mathrm{A}_\ell(P_\tau)$ and A_ℓ(SLD). In this case, only lepton universality is assumed, and no further corrections to interpret the results in terms of $\sin^2\theta_{\mathrm{eff}}^{\mathrm{lept}}$ are necessary. In the second set, consisting of $\mathrm{A}_{\mathrm{fb}}^{0,\mathrm{b}}$, $\mathrm{A}_{\mathrm{fb}}^{0,\mathrm{c}}$ and the hadronic charge asymmetry $\langle Q_{\mathrm{FB}}\rangle$, quark couplings are involved. In this case, the small non-universal flavour-specific electroweak corrections, making $\sin^2\theta_{\mathrm{eff}}^{\mathrm{lept}}$ different from that for quarks, must be taken from the SM. The effect of these corrections and their uncertainties on the extracted value of $\sin^2\theta_{\mathrm{eff}}^{\mathrm{lept}}$ is, however, negligible. The average of all six $\sin^2\theta_{\mathrm{eff}}^{\mathrm{lept}}$ determinations is:

$$\sin^2\theta_{\mathrm{eff}}^{\mathrm{lept}} = 0.23148 \pm 0.00017\,, \tag{24}$$

with a χ^2/dof of 10.2/5, corresponding to a probability of 7.0%. The enlarged χ^2/dof is solely driven by the two most precise determinations of $\sin^2\theta_{\mathrm{eff}}^{\mathrm{lept}}$, namely those derived from the measurements of A_ℓ by SLD, dominated by the left-right

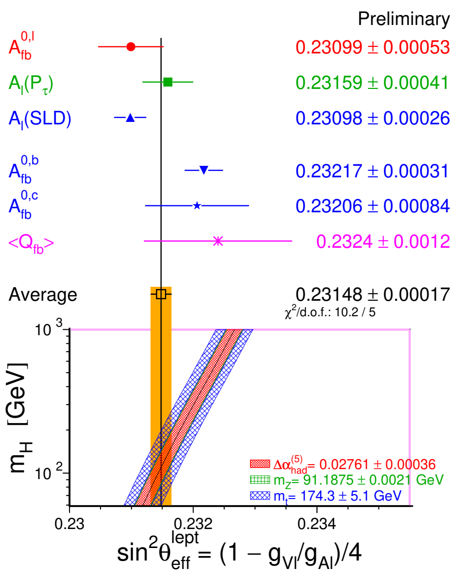

Figure 19. The effective electroweak mixing angle derived from various asymmetry measurements.

asymmetry result, and of $A_{fb}^{0,b}$ at LEP. These two measurements differ by 2.9 standard deviations. Thus, the two sets of measurements, yielding average values for $\sin^2\theta_{eff}^{lept}$ of 0.23113 ± 0.00021 ($\chi^2/dof = 1.6/2$) and 0.23217 ± 0.00029 ($\chi^2/dof = 0.05/2$), respectively, also differ by 2.9 standard deviations. This is a consequence of the same effect as discussed before: the deviation in A_b as extracted from $A_{fb}^{0,b}$ is reflected in the value of $\sin^2\theta_{eff}^{lept}$ extracted from $A_{fb}^{0,b}$.

5. W AND FOUR-FERMION PRODUCTION

In recent years many measurements pertaining to the W boson have been performed by the experiments taking data at LEP-2. The dominant production of on-shell W bosons proceeds via the CC03 process of W-pair production shown in Figure 20. The cross section of this process is measured from the kinematic threshold threshold at $\sqrt{s} = 161$ GeV up to $\sqrt{s} = 209$ GeV [18]. The preliminary combined LEP results are shown in Figure 21. Good agreement with the SM expectation is observed, showing in particular the

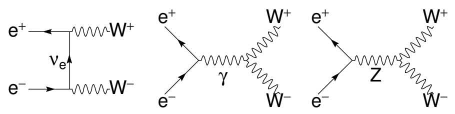

Figure 20. Lowest-order Feynman diagrams for W^+W^- production in e^+e^- interactions.

need for the triple-gauge-boson vertices γWW and ZWW. The average of the ratio of measured to predicted cross section has an accuracy of 1.1%. This accuracy requires the calculation of $\mathcal{O}(\alpha)$ radiative corrections in W-pair production [19], which lower the cross section prediction by about $(2.5 \pm 0.5)\%$. Using the Monte Carlo event generators YFSWW [20] (RacoonWW [21]) containing these corrections, a value for the ratio of 0.997 (0.999), in perfect agreement with unity, is obtained.

The $\mathcal{O}(\alpha)$ corrections also affect the differential W-pair cross section. The distribution in the polar scattering angle $\cos\theta$ becomes steeper by about 2%. With nearly 10,000 W-pair events per experiment, such a change is significant. In particular, it mimics the effects of anomalous triple-gauge-boson couplings (TGCs), which also modify the $\cos\theta$ distribution as shown in Figure 22. New TGC combinations from LEP-2 were presented at this conference which for the first time take these effects fully into account.

The TGCs considered are g_1^Z, κ_γ and λ_γ, where g_1^Z is the weak charge of the W boson, *i.e.*, it's coupling strength to the Z, and κ_γ and λ_γ are related to the magnetic dipole and electric quadrupole moment of the W boson, $\mu_W = e(1 + \lambda_\gamma + \kappa_\gamma)/(2M_W)$ and $Q_W = e(\lambda_\gamma - \kappa_\gamma)/M_W^2$, respectively. Besides W^+W^- production, additional constraints on the γWW vertex arise from single-W production, Figure 23. The cross section for this process, shown in Figure 24, is particularly sensitive to κ_γ.

The preliminary LEP-2 results are [22]:

$$g_1^Z = +0.998 \pm 0.024 \quad \text{(SM: 1)} \tag{25}$$
$$\kappa_\gamma = +0.943 \pm 0.055 \quad \text{(SM: 1)} \tag{26}$$
$$\lambda_\gamma = -0.020 \pm 0.024 \quad \text{(SM: 0)} \tag{27}$$

where each of these TGCs is determined assuming

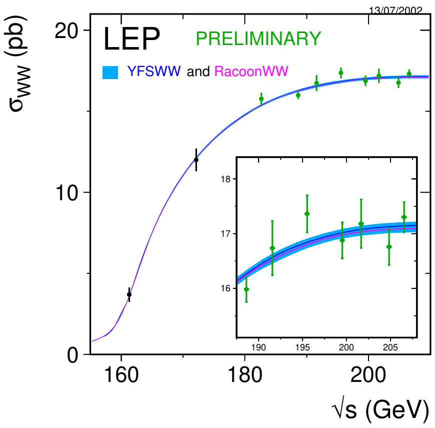

Figure 21. Measured W^+W^- cross section compared to the SM expectations.

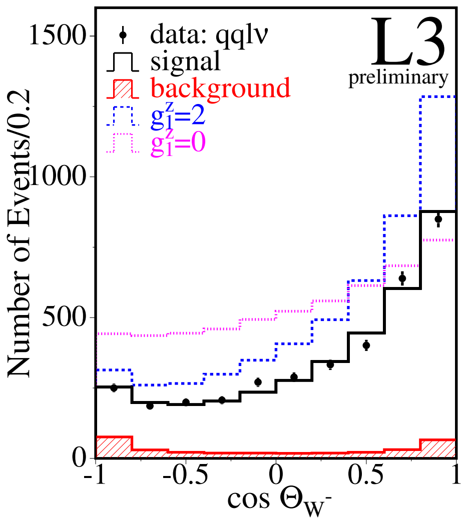

Figure 22. Polar scattering angle of the W^- boson as observed by L3 in semileptonic W-pair events compared expectations in the SM ($g_1^Z = 1$) and for anomalous TGCs ($g_1^Z = 0, 2$).

all other couplings to have their SM value. The uncertainty on the TGCs is dominated by the theoretical uncertainty on the $\cos\theta$ slope. Currently the full $\mathcal{O}(\alpha)$ correction to the slope is taken as theoretical uncertainty, amounting to about 2/3 of the total error on the TGCs. Studies are ongoing to evaluate the remaining theoretical uncer-

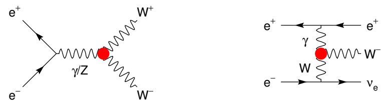

Figure 23. Some lowest order Feynman diagrams containing three-boson vertices.

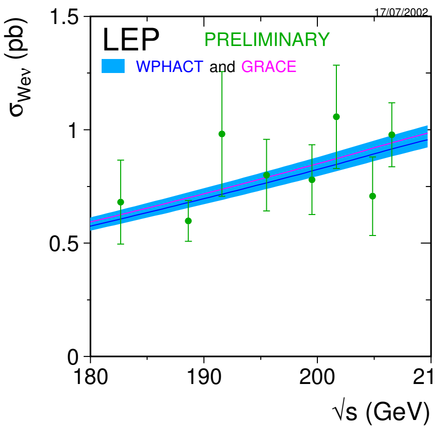

Figure 24. Measured cross section for single-W production compared to the SM expectation.

tainty on the $\cos\theta$ shape [19] and to propagate it to the TGCs.

Many more small-cross-section processes are now measured at LEP-2 [18,23], for example radiative W-pair production sensitive to quartic gauge boson couplings, Figure 25, Z-pair production or Zee production. As shown in Figure 26, such small cross sections, a factor of up to 100 smaller than that of W-pair production, are now measured with an accuracy ranging from 5% to 10% and found to be in agreement with the SM expectation. These processes allow the determination of neutral triple gauge couplings and of quartic gauge couplings [24].

6. W-BOSON MASS AND WIDTH

Until a few years ago, the W boson mass and width was measured at hadron colliders only, most recently by the experiments CDF and DØ taking data at the Fermilab proton-antiproton TEVATRON collider. Leptonic W decays with electrons and muons are selected and recon-

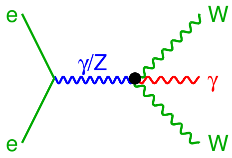

Figure 25. Lowest-order Feynman diagram in $W^+W^-\gamma$ production with a four-boson vertex.

structed. The transverse mass, *i.e.*, the invariant mass of the lepton and the missing momentum vector in the plane transverse to the beam axis is unaffected by the unknown longitudinal boost of the W boson and bounded from above by the invariant mass of the decaying W boson. The distribution of the transverse mass is shown in Figure 27. The sharp upper edge, also called Jacobian peak, yields the mass of the W boson, while the W-boson width is derived from the high-mass tail of this distribution. Final results on M_W and Γ_W from CDF and DØ are now available for the complete Run-1 data set. They are combined taking correlations properly into account [25].

Since 1996 the W boson mass and width is also measured at LEP using $e^+e^- \rightarrow W^+W^- \rightarrow f\bar{f}f\bar{f}$ events. Four-fermion final states are selected and the two decaying W bosons are reconstructed. For hadronic and semileptonic W-pair events, the W-pair kinematic is completely reconstructed so that one directly measures the invariant masses of the decaying W bosons as shown in Figure 28 [26], where the width of the mass peak is given by detector resolution and the natural width of the W boson.

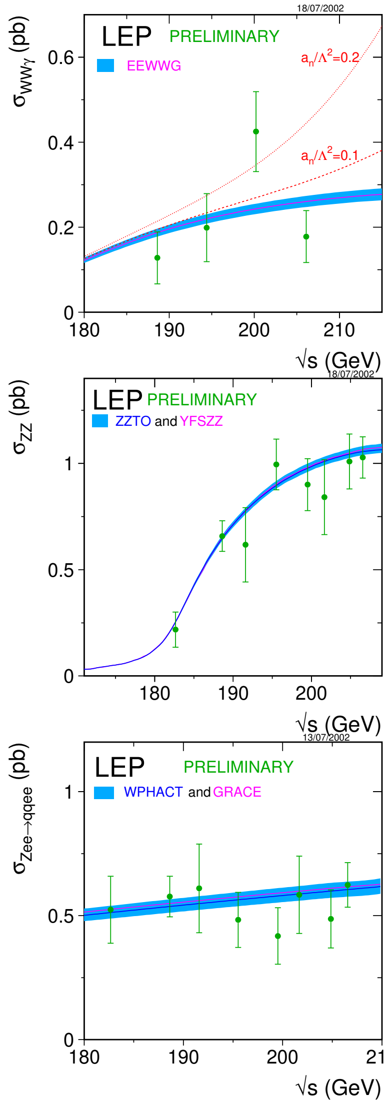

Figure 26. Measured cross sections for radiative W-pair production, ZZ and Zee production, compared to the SM expectations.

6.1. Final State Interconnection Effects

For hadronic W-pair events, $e^+e^- \rightarrow W^+W^- \rightarrow q\bar{q}q\bar{q} \rightarrow$ *hadrons*, cross talk effects may occur between the two hadronic systems as shown in Figure 29. The four-momentum exchange causes the mass of the decaying W bosons to be different from the mass of the hadronic decay products, thus leading to potentially large systematic effects.

Such final-state interconnection (FSI) effects are colour reconnection (CR), yielding a rearrangement of the colour flow in the perturbative and non-perturbative phase of the parton shower evolution, and Bose-Einstein correlations (BEC) between identical mesons in the final state. Recent analyses use the data to limit possible FSI bias on $M_W(qqqq)$.

CR [27] is searched for by studying the particle

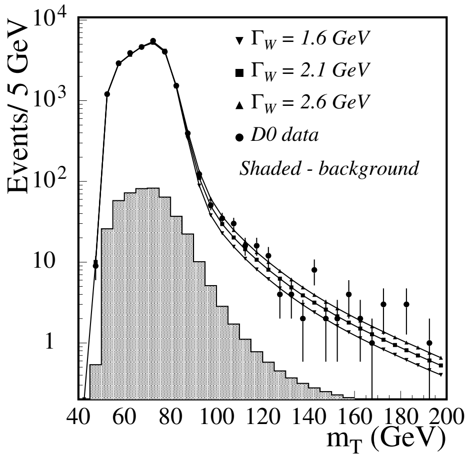

Figure 27. Transverse mass reconstructed in $W \to e\nu$ events by the DØ experiment in Run-I.

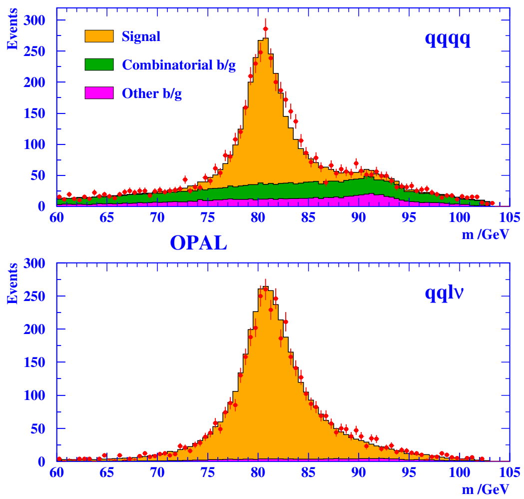

Figure 28. Invariant mass of W bosons reconstructed in (top) hadronic and (bottom) semileptonic W-pair events by the OPAL experiment.

flow in the two regions A and B between jets from the same W boson, versus that in the two regions C and D between jets originating from different W bosons, by projecting onto the planes defined by each of the regions A to D. In order to enhance the statistical sensitivity, the distributions in the intra-W regions A and B are added and

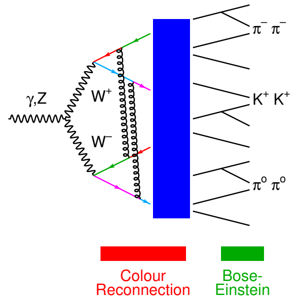

Figure 29. FSI effects: CR and BEC.

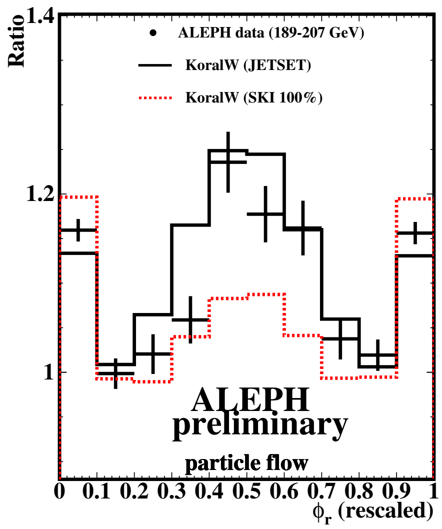

Figure 30. Ratio of particle flow distributions.

divided by the sum of the inter-W regions C and D. The ratio R=(A+B)/(C+D) is analysed as a function of the local angle between jets, as shown in Figure 30. It can be seen that CR leads to a depletion of R in the region between jets.

In order to quantify the measurement, the particle flow in A+B and in C+D is integrated over the central region between jets and the ratio is taken, yielding a single number. The result obtained on data is calibrated in sensitivity and central value to MC models incorporating different models of CR. The results of the four LEP experiments are shown in Figure 31. Combining the results of the four LEP experiments weighted by their sensitivity to a given CR model such as

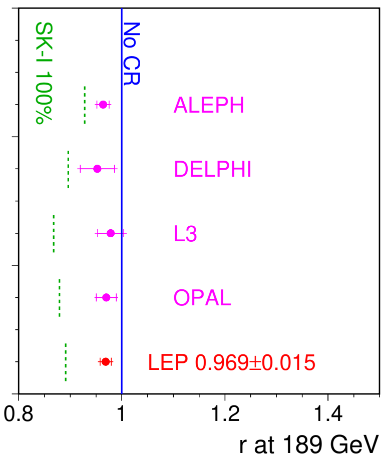

Figure 31. Ratio of the particle flow integrals as measured by the LEP experiments, compared to the expectations for no-CR and 100% CR probability in the SK-I model.

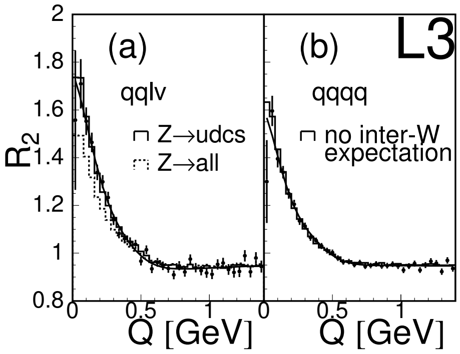

Figure 32. Rate of like-sign pairs normalised to the rate of unlike-sign pairs as a function of Q. Left: Semileptonic W-pair events compared to Z decays; right: hadronic W-pair events.

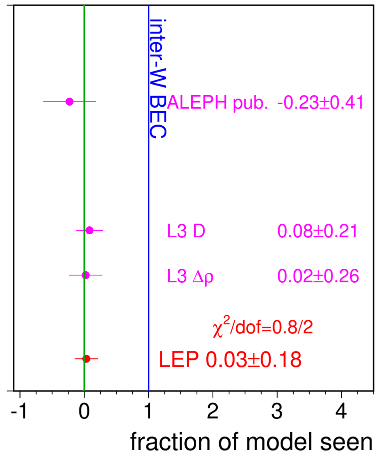

Figure 33. Measured fraction of inter-W BEC.

SK-1, one observes a small hint, at the level of 2 standard deviations off the non-CR scenario, for the presence of CR in the data, corresponding to about 40% CR in the SK-1 model.

For a given CR probability, all four experiments observe the same mass shift in the SK-I model. It is limited to be less than 90 MeV averaged over centre-of-mass energies. All other CR models yield smaller shifts. Since this preliminary result already includes most of the full LEP-2 statistics, the limit on the bias will not improve much. The solution currently under investigation is thus to use jet and event reconstruction algorithms less sensitive to CR effects, *e.g.*, to use only the core of the jets or to disregard low energy particles.

BEC [28] between identical mesons in hadronic Z decays are well established at LEP. They manifest themselves as an increased rate of pairs of identical hadrons, or simply charged tracks in the detector, which are close in phase space, *i.e.*, at low four-momentum difference Q. Indeed the strength and shape of BEC observed in the Q distribution is the same for hadronic W decays and hadronic Z decays excluding b quarks as those do not arise in W decay, as shown in Figure 32.

In order to be sensitive only to BEC between tracks from different W bosons, the BEC effects from single W bosons are divided out in the ratio D(Q). Only inter-W BEC potentially affect the W-mass reconstruction. ALEPH and L3 do not find any sign of inter-W BEC, with the combined result being that $(3 \pm 18)\%$ of the full effect of inter-W BEC is observed, Figure 33, in good agreement with zero. This corresponds to a bias on $M_{\mathrm{W}}(qqqq)$ of less than 10 MeV at 68% CL, while the full effect would correspond to about 35 MeV for this particular model.

However, the new preliminary DELPHI analysis observes an effect in the D(Q) distribution

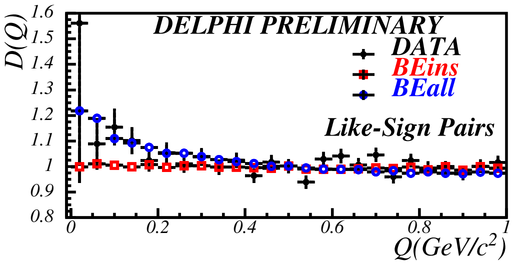

Figure 34. D(Q) sensitive to inter-W correlations only as measured by the DELPHI collaboration.

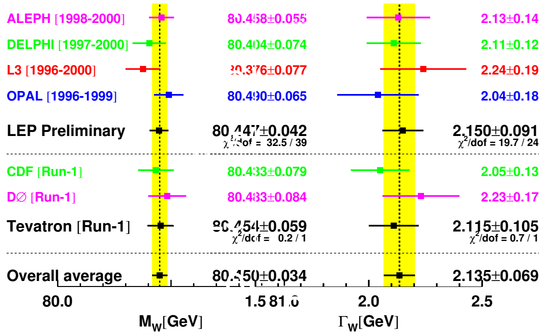

Figure 35. Results on M_{W} and Γ_{W} obtained from the six TEVATRON and LEP experiments.

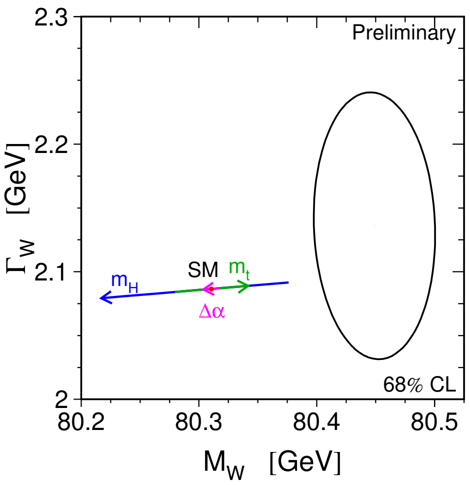

Figure 36. Contour curves of 68% probability in the $(M_{\mathrm{W}}, \Gamma_{\mathrm{W}})$ plane. The SM expectation is shown as the arrow for $M_{\mathrm{t}} = 174.3 \pm 5.1$ GeV and $M_{\mathrm{H}} = 300^{+700}_{-186}$ GeV.

as shown in Figure 34, with a significance of 2.8 standard deviations away from zero. Both results differ by about two standard deviations. Studies are ongoing to understand the different observations.

Based on the above studies, uncertainties of 90 MeV for CR and 35 MeV for BEC are assigned to the mass of the W boson as extracted from the four jet channel. Because of these large additional uncertainties compared to the semileptonic channel, the weight of the four jet channel in the LEP average is less than 10%. The difference in mass obtained for hadronic and semileptonic W-pair events, calculated without FSI uncertainties, is (9 ± 44) MeV, well compatible with zero.

6.2. Results

The results of the six TEVATRON and LEP experiments on the mass and the width of the W boson are shown in Figure 35. Excellent agreement is observed. The combined results and their correlation is shown in Figure 36, together with the SM expectation. It can be seen that the W mass is highly sensitive to SM parameters, in particular preferring a low value for the mass of the Higgs boson.

7. TESTS OF THE STANDARD MODEL

Within the framework of the SM, each of the observables presented above are calculated as a function of five main relevant parameters, which are the running electromagnetic and strong coupling constant evaluated at the Z pole, $\Delta\alpha^{(5)}_{had}$ and α_S, and the masses of Z boson, top quark and Higgs boson, M_{Z}, M_{t}, M_{H}. Using the Fermi constant G_{F} allows to calculate the mass of the W boson. The running electromagnetic coupling is represented by the hadronic vacuum polarisation $\Delta\alpha^{(5)}_{had}$, as it is this contribution which has the largest uncertainty, similar to the case of the muon anomalous magnetic moment.

The precision of the Z-pole measurements require matching precision of the theoretical calculations, first and second order electroweak and QCD corrections etc. The dependence on M_{t} and M_{H} enters through radiative corrections as

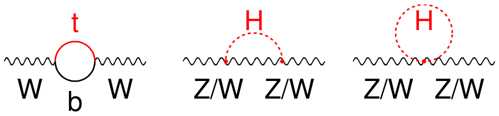

Figure 37. W and Z propagator corrections involving the top quark and the Higgs boson.

depicted in Figure 37. The computer programs TOPAZ0 [29] and ZFITTER [30], incorporating state-of-the-art calculations, are used to calculate the predictions as a function of the five SM parameters. For the hadronic vacuum polarisation, the result $\Delta\alpha^{(5)}_{had} = 0.02761 \pm 0.00036$ [31], based on the recent BES measurements [32], is used.

Using the Z-pole measurements of SLD and LEP-1 in order to evaluate electroweak radiative corrections, the masses of two heavy particles measured at the TEVATRON and at LEP-2, namely the top quark and the Higgs Boson, can be predicted. The resulting 68% C.L. contour in the $(M_{\rm t}, M_{\rm W})$ plane is shown in Figure 38. Also shown is the contour corresponding to the direct measurements of both quantities at the TEVATRON and at LEP-2. The two contours overlap, successfully testing the SM at the level of electroweak radiative corrections. The diagonal band in Figure 38 shows the constraint between the two masses within the SM, which depends on the mass of the Higgs boson, and to a small extend also on the hadronic vacuum polarisation (small arrow labelled $\Delta\alpha$). Both the direct and the indirect contour prefer a low value for the mass of the SM Higgs boson.

The best constraint on $M_{\rm H}$ is obtained by analysing all data. This joint fit has a χ^2 of 29.7 for 15 degrees of freedom, corresponding to a probability of only 1.3%. The pulls of the 20 measurements entering the fit are shown in Figure 39. The single largest contribution to the χ^2, 9 units, arises from the NuTeV measurement of the on-shell electroweak mixing angle. Excluding the NuTeV measurement, the χ^2/dof becomes 20.5/14, corresponding to 11.4%. The fitted parameters in terms of central value and error are almost unchanged, showing that the fit is robust against the NuTeV result.

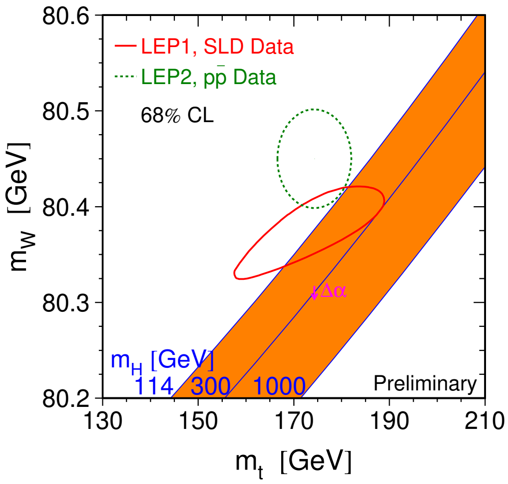

Figure 38. Contours of 68% probability on the $(M_{\rm t}, M_{\rm W})$ plane, for the corresponding direct and the indirect determinations. Also shown is the correlation between $M_{\rm W}$ and $M_{\rm t}$ as expected in the minimal SM for different Higgs boson masses.

The global fit yields $M_{\rm H} = 81^{+52}_{-33}$ GeV, which corresponds to a one-sided upper limit at 95% C.L. on $M_{\rm H}$ of 193 GeV including theory uncertainty as shown in Figure 40. The fitted $M_{\rm H}$ is strongly correlated with the hadronic vacuum polarisation (correlation of -0.48) and the fitted top-quark mass (0.70). The strong correlation with $M_{\rm t}$ implies a shift of 35% in the predicted $M_{\rm H}$ if the measurement of $M_{\rm t}$ changes by one standard deviation ($5\ GeV$). Thus a precise experimental measurement of $M_{\rm t}$ is very important.

Also shown are the χ^2 curves obtained with theory-driven and thus more precise evaluation of the hadronic vacuum polarisation [33], or excluding the NuTeV result. Both yield nearly the same upper limits on $M_{\rm H}$. The theoretical uncertainty on the SM calculations of the observables is visualised as the thickness of the blue band. It is dominated by the theoretical uncertainty in the calculation of the effective electroweak mixing angle, for which a complete two-loop calculation is still lacking.

Also shown in Figure 40 is the $M_{\rm H}$ range excluded by the direct search for the Higgs boson, discussed in the following section. Even though

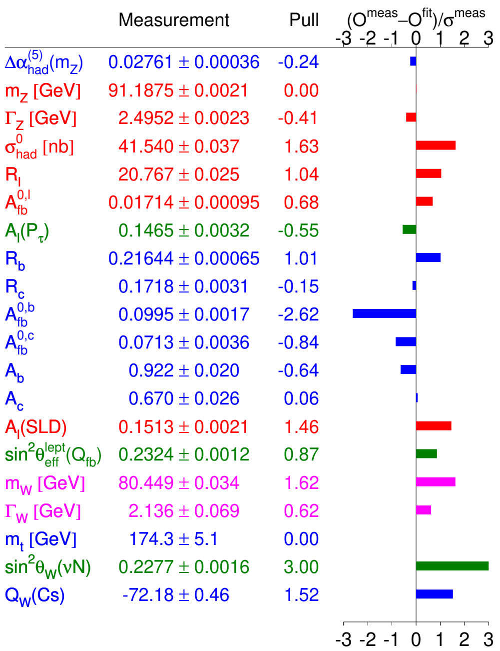

Figure 39. Pulls of all 20 measurements used in the global SM analysis. The pull is the difference between measured and expected value calculated for the minimum of the χ^2, divided by the measurement error.

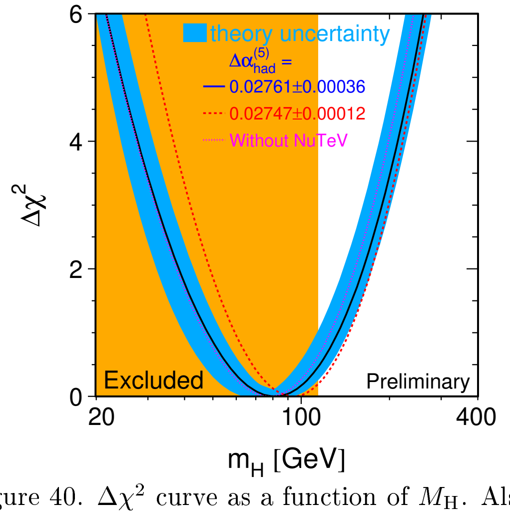

Figure 40. $\Delta\chi^2$ curve as a function of M_H. Also shown are the curves using a theory-driven evaluation of the hadronic vacuum polarisation, or excluding the NuTeV measurement.

the minimum of the χ^2 curve lies in the excluded region, the uncertainties on the Higgs mass value are such as that the results are well compatible.

8. DIRECT HIGGS-BOSON SEARCH

Only the direct observation of the Higgs boson constitutes a proof of its existence; the indirect constraint on the Higgs boson mass already assumes that the SM Higgs boson actually exists. Direct searches for the Higgs Boson have been carried out by the LEP experiments, with the final results from LEP-2 now available [34].

Higgs production at LEP occurs dominantly through radiation of a Higgs Boson off an s-channel produced Z boson, $e^+e^- \to ZH \to f\bar{f}b\bar{b}$, yielding a four-fermion final state. Smaller contributions to the cross section arise through WW and ZZ fusion especially for Higgs masses beyond the nominal kinematic limit of ZH production.

The analysis combines Higgs-mass independent selections with Higgs-mass reconstruction. For increasingly pure selections, the distribution of reconstructed candidate Higgs boson masses is shown in Figure 41, with a small accumulation of events at about 115 GeV.

The complete statistical analysis for the direct search is based on a global discriminating variable, which combines all event information and separates between signal and background events, and the reconstructed Higgs mass. Figure 42 shows the confidence level for the hypothesis of the observed data being SM background only, as a function of hypothetical Higgs masses. The largest excess over background at high masses shows a significance of 1.7 standard deviations, corresponding to a probability for a background fluctuation of 8%, at masses around 115 to 117 GeV. This small excess is solely given by one experiment, ALEPH, where the significance is about 2.8-3.0 standard deviations, and in one channel only, namely qqbb.

Without evidence for direct Higgs production in the LEP combined data set, the data are used to set a lower limit on the mass of the SM Higgs boson of 114.4 GeV at 95% C.L. Because of the small excess, the observed limit is 0.9 GeV smaller than the expected limit.

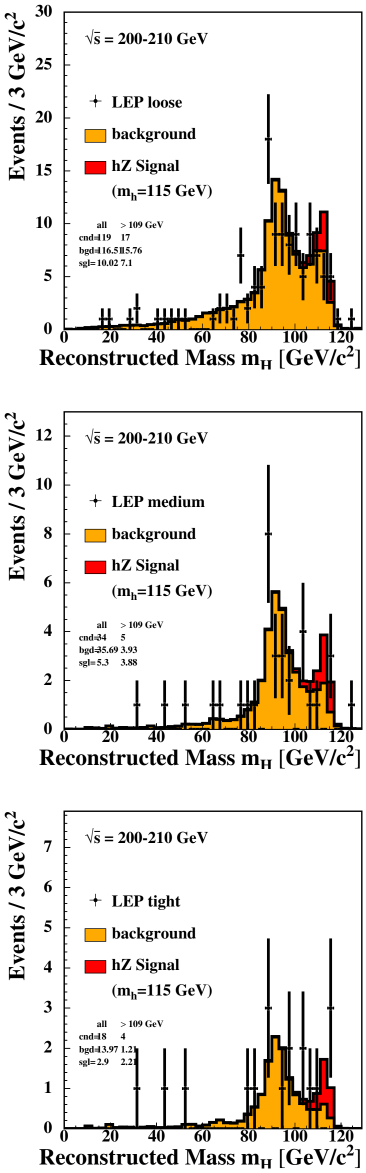

Figure 41. Reconstructed Higgs mass in ZH candidates selected by the four LEP experiments, for increasing purity of the selection.

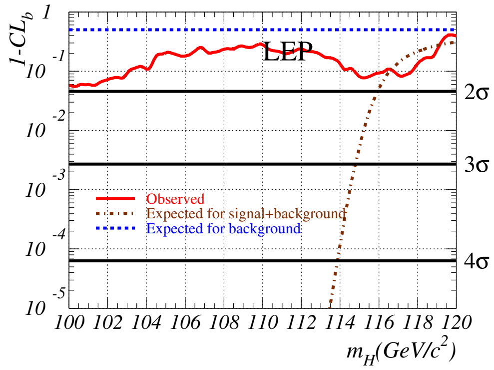

Figure 42. Confidence level for the background-only hypothesis.

9. OUTLOOK

Since 2001, Run-II of data taking at the TEVATRON is ongoing. The proton-antiproton centre-of mass energy is raised from 1.8 TeV to 1.96 TeV. Each experiment will collect about 15/fb in total, and about 2/fb up to 2004 [35,36]. Among other things, this will allow measurements of M_{W} with an accuracy of 25 MeV and of M_{t} with an accuracy of 2.5 GeV, yielding a Higgs mass prediction based on electroweak radiative corrections of 30% accuracy. Besides the width of top quark and W boson, also gauge couplings will be measured with high precision. An interesting aspect concerns Z production with subsequent decay into lepton pairs. This process allows to reconstruct the centre-of-mass system and thus the forward-backward asymmetry in this system, which is a measurement of the effective electroweak mixing angle. The estimated precision is in the range of current Z-pole determinations of $\sin^2\theta_{\mathrm{eff}}^{\mathrm{lept}}$, thus would be useful to shed light on the dispersion of the various existing measurements of that quantity. Crucial for this measurement are precise matrix elements and parton distribution functions including theoretical uncertainties. Constraints on these could also be determined from W production data.

The TEVATRON experiments will perform the next step in the direct search for the Higgs boson. With 15/fb per experiment, the two experiments will be sensitive to Higgs masses of up to 135 GeV at the level of three standard deviations, well beyond the existing limit.

10. CONCLUSION

During the last decade many experiments, such as BES, E821, NuTeV, SLD, ALEPH, DELPHI, L3, OPAL, CDF and DØ, etc. have performed a wealth of measurements of unprecedented precision in particle physics. These measurements test all aspects of the SM of particle physics, and many of them show large sensitivity to electroweak radiative corrections at loop level.

Most measurements agree with the expectations as calculated within the framework of the SM, successfully testing the SM at Born and at loop level. Still there are two "3 standard deviations effects", namely the spread in the various determinations of the effective electroweak mixing angle, and NuTeV's result, most pronounced when interpreted in terms of the on-shell electroweak mixing angle.

For the experiments at current and future colliders, precise theoretical calculations are needed, which must include an assessment of the remaining theoretical uncertainty [19,37–39]. The required precision must match the expected experimental precision in measurements of observables such at the masses of top quark and W boson, the effective electroweak mixing angle and the hadronic vacuum polarisation based on low-energy data.

The next qualitative step is surely given by the observation of the SM Higgs boson or a Higgs boson of any other model. Searches will be performed at TEVATRON, while experiments at future linear colliders [40] and notably the LHC [41] will be sufficiently powerful to find the Higgs boson or indications of other mechanisms of electroweak symmetry breaking.

11. ACKNOWLEDGEMENTS

It is a pleasure to thank my colleagues of the TEVATRON and LEP electroweak working groups, members of the BES, E821, NuTeV, SLD, ALEPH, DELPHI, L3, OPAL, CDF and DØ experiments, as well as D. Bardin, P. Gambino, G. Passarino and G. Weiglein for valuable discussions.

REFERENCES

1. H.N. Brown *et al.*, PRL 86 (2001) 2227.
2. S. Davidson *et al.*, JHEP 02 (2002) 37.
3. M. Knecht *et al.*, PRD 65 (2002) 073034, PRL 88 (2002) 071802.
4. Y. Semertzidis, *these proceedings.*
5. G.W. Bennett *et al.*, hep-ex/0208001.
6. T. Teubner, *these proceedings.*
7. K. Hagiwara *et al.*, hep-ph/0209187.
8. M. Davier *et al.*, hep-ph/0208177.
9. E. Paschos, L. Wolfenstein, PRD 7 (1973) 91.
10. G.P. Zeller *et al.*, PRL 88 (2002) 091802.
11. K.S. McFarland, proceedings 28th ICHEP, Warsaw, Poland (1996); M. Goncharov *et al.*, PRD 64 (2001) 112006.
12. P. Gambino, *these proceedings.*
13. The LEP Collaborations, hep-ex/0101027.
14. I. De Bonis, *these proceedings.*
15. K. Miyabayashi *et al.*, PLB 347 (1995) 171.
16. K. Yusa *et al.*, PLB 447 (1999) 167.
17. R. Hawkings, *these proceedings.*
18. L. Malgeri, *these proceedings.*
19. W. Placzek, *these proceedings.*
20. S. Jadach *et al.*, CPC 140 (2001) 432.
21. A. Denner *et al.*, PLB 475 (2000) 127.
22. S. Jezequel, *these proceedings.*
23. E. Migliore, *these proceedings.*
24. S. Wynhoff, *these proceedings.*
25. S. Eno, *these proceedings.*
26. J. Nowell, *these proceedings.*
27. E. Bouhova-Thacker, *these proceedings.*
28. S. Todorova-Nova, *these proceedings.*
29. G. Passarino *et al.*, CPC 117 (1999) 278.
30. D. Bardin *et al.*, CPC 133 (2001) 229.
31. H. Burkhardt, B. Pietrzyk, PLB 513 (2001) 46.
32. Z. Zhao, *these proceedings.*
33. J.F. de Troconiz, F.J. Yndurain, PRD 65 (2002) 093002
34. C. Mariotti, *these proceedings.*
35. I. Iashvili, *these proceedings.*
36. D. Glenzinski, *these proceedings.*
37. S. Jadach, *these proceedings.*
38. G. Passarino, *these proceedings.*
39. J. Kühn, *these proceedings.*
40. A. Sopczak, *these proceedings.*
41. F. Piccininni, *these proceedings.*